Design and exploitation of a vorticity probe for turbulence studies in fusion devices

Sérgio Caramona
sergio.caramona@ist.utl.pt

Instituto Superior Técnico, Lisboa, Portugal

September 2020

Abstract

Understanding the generation mechanism of anomalous flows presents itself as a big challenge in fusion. During this work, the impact of turbulent regimes in the outer regions of the plasma in the overall plasma confinement is highlighted. This particle and energy turbulent flux usually comes in the form of coherent structures, also called eddies, that seems to be generated by the change in topology from closed to open magnetic field lines, around the Scrape off Layer. Recurring to a Langmuir probe array, specifically designed to acquire floating potentials and ionic saturation currents it is possible to infer some turbulence physical properties, with a special focus on the vorticity, a quantity that was still not extensively explored from an experimental point of view. A detailed statistical description of these quantities highlights the interplay between fluctuations in gradients and turbulent transport. The influence of polarization on global and edge plasma parameters is studied with a negative bias induced by an emissive electrode. The effects of higher magnetic field configurations on tokamaks is also explored.

Keywords: Nuclear fusion, Vorticity, Reynolds Stress, Particle flux, Poloidal velocity

1. Introduction

Plasmas in fusion research are far from thermodynamic equilibrium, which leads to a dynamical behavior and the formation of structures that affect the transport mechanisms. Spatial variations of quantities like density, temperature, the intensity of the magnetic field or external force fields create instabilities, with the properties of plasma changing dramatically, leading to anomalous transport. These mechanisms constitute themselves as one obstacle to achieving ignition in magnetically confined plasmas. The SOL(scrape-off layer) region constitute only a small portion of the tokamak device in terms of geometrical dimensions and heat content. Although, this small region influences the global confinement significantly with sharp variations in the gradients of some plasma parameters as: temperature, floation potential or density. During the past decades, studies in this region shifted towards a non stationary/intermittent approach for edge turbulence[4]. Edge and SOL plasmas are usually characterized by a large amplitude of turbulent fluctuations with an associated enhanced transport in walls direction. Predicting SOL dynamics is one of the main challenges in fusion, since SOL physics determines the boundary conditions for the plasma across the machine, regulating the power losses.

2. Background

2.1. Vorticity

Vorticity can be defined as the curl of $\vec{v}$, the flow velocity:

$$w = \nabla \times \vec{v} \tag{1}$$

Replacing the flow velocity by the fluctuations of the $E \times B$ velocity $\vec{v}_{E\times B} = \frac{\vec{E}\times\vec{B}}{B^2}$ and approximating the electric field to the electrostatic fluctuation, the vorticity can be written as:

$$\tilde{w} = \frac{\partial v_\theta}{\partial r} - \frac{\partial v_r}{\partial \theta} = \frac{1}{B}\nabla^2\tilde{\phi} \tag{2}$$

where $\nabla^2\tilde{\phi}$ corresponds to the Poison equation, v_r and v_θ are given by equation $\tilde{v}_r = \frac{\nabla_\theta\tilde{\phi}}{B} \propto \frac{\tilde{E}_\theta}{B}$ and $\tilde{v}_\theta = \frac{\nabla_r\tilde{\phi}}{B} \propto \frac{\tilde{E}_r}{B}$ respectively.

Vorticity is a vector field that gives a microscopic measure of the rotation at any point in the fluid.

Discretizing equation 2, using a finite difference approximation:

$$\frac{\partial\phi}{\partial x} \approx \frac{\phi(x+h) - \phi(x-h)}{2h} \tag{3a}$$

$$\frac{\partial^2\phi}{\partial x^2} \approx \frac{\phi(x+h) - 2\times\phi(x) + \phi(x-h)}{h^2} \tag{3b}$$

The vorticity can be then written as:

$$\tilde{w} = \frac{1}{B}\left(\frac{\tilde{\phi}(x+h) - 2\times\tilde{\phi}(x) + \tilde{\phi}(x-h)}{\Delta x^2} + \frac{\tilde{\phi}(y+h) - 2\times\tilde{\phi}(y) + \tilde{\phi}(y-h)}{\Delta y^2}\right) \quad (4)$$

Where the left term of Equation 4 is related to x coordinates of the probe and the right side to the y coordinates.

The vorticity flux can be calculated from the relation between the vorticity and the radial $E \times B$ velocity component:

$$\Gamma_w = \langle \tilde{v}_r . \tilde{w} \rangle \propto \frac{\left\langle -\tilde{E}_\theta . \tilde{w} \right\rangle}{B} \quad (5)$$

2.2. Reynolds Stress

A turbulent flow is defined as the flow in which the system's inertial forces are dominant over the viscous forces. This phenomenon is described by Reynolds number that determines when the turbulent flow will occur. In the context of fusion, the Reynolds stress may give a measure of the self-consistent flow generation in plasmas by the small-scale turbulent fluctuations[11], responsible for the generation of radial electric fields. It is suggested that the radially varying Reynolds stress may play an important role in the generation of sheared poloidal flows[8][1].

The Reynolds stress (Re) can be approximated by:

$$Re \approx \langle \tilde{v}_r \tilde{v}_\theta \rangle \quad (6)$$

The velocity terms of the Reynolds stress tensor are related to the $E \times B$ velocity $\langle \tilde{v}_r \tilde{v}_\theta \rangle \propto \left\langle \tilde{E}_r \tilde{E}_\theta \right\rangle$, where $\tilde{E}_r$ and $\tilde{E}_\theta$ are the radial and poloidal components of the electric field respectively. The Reynolds stress can then be rewritten as follows:

$$Re \propto \frac{1}{B^2}\left\langle \tilde{E}_r \tilde{E}_\theta \right\rangle \quad (7)$$

A non-zero value of the gradient Reynolds stress can drive a laminar flow. The correlation needed between v_r and v_θ (or in the electric field components) occurs naturally in the presence of a background gradient driving turbulent transport. Evidence of the importance of Reynolds stress in fusion was found in ISTTOK, using a Langmuir probe array [5], with the vortex structures being able to transport particles, carry polarization charge and organize large-scale potential differences with induction flows perpendicular to the background density gradient [3].

2.3. Effects of polarization on SOL transport

The influence of polarization on global and edge plasma parameters is described in previous studies at ISTTOK tokamak [12].

Although both negative and positive bias reveals a large radial electric field induced by the emissive electrode and a substantial increase in plasma density, improvements in confinement are mostly observed for a negative induced bias [12]. Positive polarization seems to be related to large-amplitude fluctuations which lead to low shear induced in the edge region. These large amplitude fluctuations are suggested as the cause for the distinctive behavior between the positive and negative biasing on plasma confinment.

2.4. Poloidal phase velocity

Spatial Fourier transforms allow to compute quantities like the wave vector k, coherence between signals and even the phase velocity of these fluctuations near specific positions.

The presented method computes the plasma velocity with *S(k,w)* as the local wavenumber and frequency spectral density, estimated from two fixed probes[9]. The technique involves sampling the cross power spectrum from the probes separated at a known distance and reconstruct the wave number frequency plane, which can be integrated to obtain the spatial spectrum[10].

The sample power value $S^j(w)$ from probe n is defined using the Fourier series coefficients of the signal and its conjugate:

$$S_n^j = \Phi^{j*}(x_1, \omega)\Phi^j(x_1, \omega) \quad (8)$$

Which allows to compute the local wavenumber and frequency spectrum $S_l(k, w)$ as the sum of the sample power values at a fixed frequency and with wavenumber in the range K to $K + \Delta K$ divided by the number of records:

$$S_l(k, w) = \frac{1}{M}\sum_{j=1}^{M} I_{0,\Delta K}[K - K^j(w)]\frac{1}{2}[S_1(w) + S_2(w)] \quad (9)$$

The averaging of the two sample powers introduces more statistical value.

The function $I_{0,\Delta K}$ at 9 correspond to an algorithm that computationally can be implemented as a weighted histogram where the bins are defined with the Freedman–Diaconis rule[7] to select the optimal bin width.

The poloidal phase velocity, which can be seen as a integration of the wavenumber-frequency plane, can finally be computed as:

$$v_{phase} = \frac{\sum S(k, w)(w/k)}{\sum S(k, w)} \quad (10)$$

Using data from two probes, varying its radial position allow to determine the radial variation of the poloidal phase velocity.

The poloidal phase velocity results obtained from the wavenumber and frequency spectra method will

be compared with another procedure, recurring to correlation relations.

The cross-correlation is a measure of similarity of two time series as a function of the displacement of one relative to the other, given by:

$$G_{xy}(\tau) = \int_0^t x(t)y(t+\tau)dt \tag{11}$$

The cross correlation maximum indicates the point in time where the signals have a synchronous pattern, with the time delay between two signals determined by:

$$\tau_{delay} = arg\ max((f \star g)(t)) \tag{12}$$

3. Implementation

3.1. Vorticity probe array design/Experimental setup

The Langmuir electrostatic probes consist of insulated wires exposed to the plasma, a simple and inexpensive diagnostic to analyze tokamak edge plasmas. The design of the multi-pin probe array can have a variety of different arrangements, depending on the problem under study. The diagnostic system was designed on Autodesk Fusion360 and the manufacturing was in charge of Núcleo de Oficinas (NOF) at IST.

Equation 3b clearly suggests a design that involves a diamond shape pattern, with three different poloidally located tips at the same radial position and two tips separated radially for the vorticity measurement. Another pin is then needed to obtain the ion current saturation. The schematic of the probe is shown in figure 1 and 2.

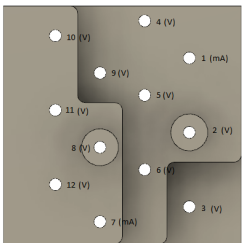

Figure 1: Vorticity probe top view.Tungsten filament not included

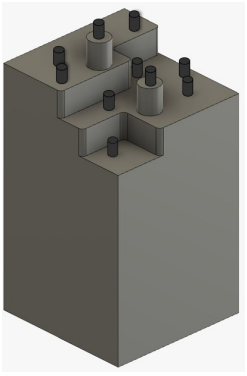

Figure 2: Vorticity probe side view.

The probe array was designed to prevent the appearance of shadows between pins. The body of the probe is built in Boron Nitrate, an insolating chemical compound characterized by its hardness (only inferior to diamond), excellent thermal and chemical stability and high conductivity. These features make the material ideal for enduring the hostile ambient inside the tokamak. The probe tips are made of tungsten filaments, a material with remarkable robustness associated with a high melting point. The probe array was designed as small as possible in order to cause the minimum interference with the plasma, with a poloidal separation Δ_θ of 5mm and a radial separation Δ_r of 3mm, as shown in figure 1 and 2. The tungsten pins have a 0.7mm diameter.

The vorticity probe described previously, acquires floating potentials and ion saturation current signals.

The radial and poloidal electric field can be respectively deduced from the gradient of floating potential signals by the following relations:

$$\begin{aligned} \tilde{E}_{r1} &= -\frac{\tilde{\phi}_3 - \tilde{\phi}_2}{\Delta r} \\ \tilde{E}_{r2} &= -\frac{\tilde{\phi}_9 - \tilde{\phi}_8}{\Delta r} \end{aligned} \tag{13}$$

$$\begin{aligned} \tilde{E}_{\theta 1} &= \frac{\tilde{\phi}_4 - \tilde{\phi}_5}{\Delta\theta} \\ \tilde{E}_{\theta 2} &= \frac{\tilde{\phi}_5 - \tilde{\phi}_6}{\Delta\theta} \\ \tilde{E}_{\theta_{T1}} &= \frac{\tilde{E}_{\theta 1} + \tilde{E}_{\theta 2}}{2} \end{aligned} \tag{14}$$

From the previous equations, the particle fluxes due to the electrostatic fluctuations, can be rewritten as:

$$\begin{aligned} \Gamma_{r1} &\propto < \tilde{n}.\tilde{V}_{E_r} > \propto \frac{\tilde{I}_{sat1}.\tilde{E}_{\theta_{T1}}}{B} \\ \Gamma_{r2} &\propto \frac{\tilde{I}_{sat2}.\tilde{E}_{\theta_{T2}}}{B} \end{aligned} \tag{15}$$

assuming that the ion saturation current is proportional to the density fluctuation[6].

The Reynolds stress, stated at equation 7 can be formulated as:

$$\begin{aligned} Re_1 &\propto \frac{1}{B^2}\left\langle \tilde{E}_r \tilde{E}_\theta \right\rangle = \frac{1}{B^2}\left(\left\langle \frac{\frac{\tilde{\phi}_4 - \tilde{\phi}_5}{\Delta\theta} + \frac{\tilde{\phi}_5 - \tilde{\phi}_6}{\Delta\theta}}{2} . \frac{-(\tilde{\phi}_3 - \tilde{\phi}_2)}{\Delta r} \right\rangle\right) \\ Re_2 &\propto \frac{1}{B^2}\left(\left\langle \frac{\frac{\tilde{\phi}_{12} - \tilde{\phi}_{11}}{\Delta\theta} + \frac{\tilde{\phi}_{11} - \tilde{\phi}_{10}}{\Delta\theta}}{2} . \frac{-(\tilde{\phi}_9 - \tilde{\phi}_8)}{\Delta r} \right\rangle\right) \end{aligned} \tag{16}$$

The floating potential signals allow to calculate the vorticity derived in section 2:

$$\begin{aligned} \tilde{w}_1 &= \frac{1}{B}\left(\frac{\tilde{\phi}_2 - 2\times\tilde{\phi}_5 + \tilde{\phi}_3}{(\Delta r)^2} + \frac{\tilde{\phi}_6 - 2\times\tilde{\phi}_5 + \tilde{\phi}_4}{(\Delta r)^2}\right) \\ \tilde{w}_2 &= \frac{1}{B}\left(\frac{\tilde{\phi}_8 - 2\times\tilde{\phi}_{11} + \tilde{\phi}_9}{(\Delta r)^2} + \frac{\tilde{\phi}_{10} - 2\times\tilde{\phi}_{11} + \tilde{\phi}_{12}}{(\Delta r)^2}\right) \end{aligned} \tag{17}$$

The vorticity result allow to rewrite the vorticity flux expressed at equation 5 as:

$$\begin{aligned} \Gamma_{w1} &= \frac{1}{B}\left(\left\langle \alpha . \frac{\beta}{B} \right\rangle\right) \\ \Gamma_{w2} &= \frac{1}{B}\left(\left\langle \zeta . \frac{\delta}{B} \right\rangle\right) \end{aligned} \tag{18}$$

with:

$$\alpha = \left(\frac{\frac{\tilde{\phi}_4 - \tilde{\phi}_5}{\Delta\theta} + \frac{\tilde{\phi}_5 - \tilde{\phi}_6}{\Delta\theta}}{2} \right)$$
$$\beta = \left(\frac{\tilde{\phi}_2 - 2 \times \tilde{\phi}_5 + \tilde{\phi}_3}{(\Delta r)^2} + \frac{\tilde{\phi}_6 - 2 \times \tilde{\phi}_5 + \tilde{\phi}_4}{(\Delta r)^2} \right)$$
$$\zeta = \left(\frac{\frac{\tilde{\phi}_{12} - \tilde{\phi}_{11}}{\Delta\theta} + \frac{\tilde{\phi}_{11} - \tilde{\phi}_{10}}{\Delta\theta}}{2} \right)$$
$$\delta = \left(\frac{\tilde{\phi}_8 - 2 \times \tilde{\phi}_{11} + \tilde{\phi}_9}{(\Delta r)^2} + \frac{\tilde{\phi}_{10} - 2 \times \tilde{\phi}_{11} + \tilde{\phi}_{12}}{(\Delta r)^2} \right) \quad (19)$$

4. Results

The experiments were performed with 3 different tokamak configurations. The first one, which will be presented in detail through this article, consists of experiments with a magnetic field of 0,5 Tesla with the Plasma controlled using PID techniques. The second configuration was similar, but the polarization device was removed. The third has a higher magnetic field, with a value of 0.6 Tesla. Signals from probe array 2 will be presented for this work in particular. The limiter position corresponds to the value of x=0 in all figures exhibited, with negative x values inside the limiter and positive in the SOL region. Results for the first experiment are highlighted. For the full three experiment analysis review [13].

4.1. Floating potential and ion current saturation profiles

The presented floating potential and ion current profiles are obtained averaging the regions of the cycles under study for each probe.

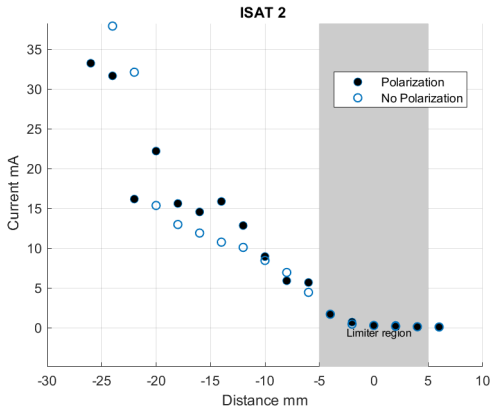

Figure 3: Ion current saturation profile from pin 7. Positive Cycle.

Both ion current saturation values show in Figure 3 an increase as we move towards the tokamak inner positions. The probe starts to collect current around the position 5 millimeters inside the limiter, with a stronger variation observed in both probes around the position 20 millimeters. Signals with polarization have saturation currents slightly smaller, compared with signals without polarization in the innermost regions.

The floating potential profiles for the remaining probes are also computed. These results were computed for all the cycles under study. An example of a floating potential profile is shown in Figure 4:

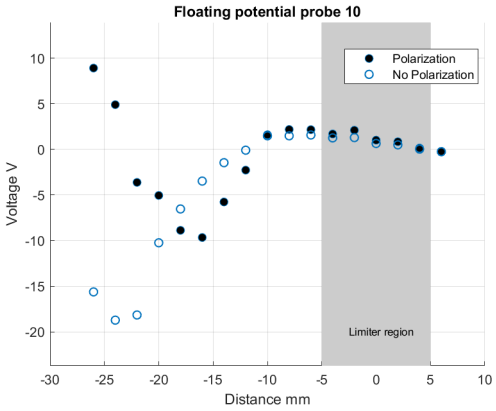

Figure 4: Floating potential radial profile from pin 10. Positive Cycle.

From previous experiments and knowledge of plasma behavior in tokamaks, a constant increase in the floating potentials, and ion current, moving to the inland regions of the tokamak, is expected. Some floating potential profiles show an unexpected behavior, especially in the innermost regions of the tokamak. The profiles for the polarization results show floating potential profiles close to zero before 10 millimeters, dropping continuously until 15 millimeters, increasing in the inner regions of the tokamak. The results for the higher magnetic field experiment show values close to the ones obtained for the polarization in the first experiment. A second series of experiments, this time without the electrode inside the tokamak were performed. The radial profiles obtained are comparable to the ones from the first experiment.

4.2. Electric Fields

The radial and poloidal electric field results for probe two are presented in Figure 5 and 6 respectively. Probe 1 yields comparable results.

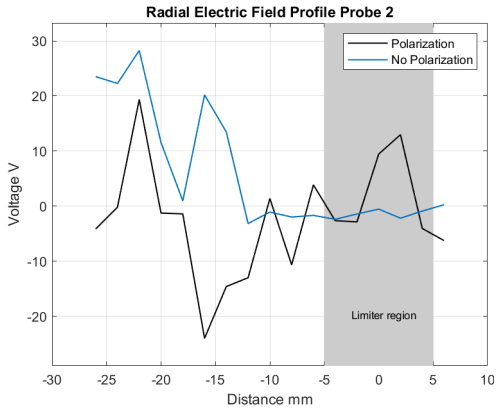

Figure 5: Radial electric field profile for probe 2. Positive Cycle.

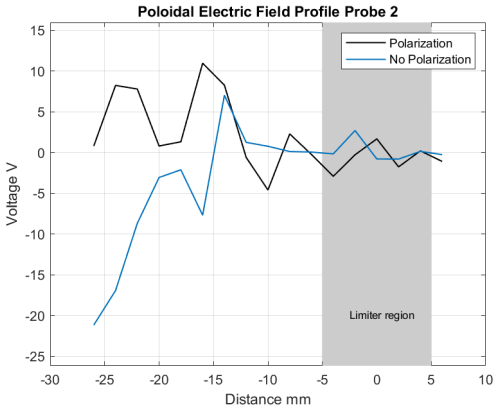

Figure 6: Poloidal electric field profile for probe 2. Positive Cycle.

The electric field for both probes is close to zero in the SOL region for the nonpolarized signals analyzed. Polarization increases the oscillation of the electric field in this region. There is evidence of a shear layer around the region 10/15 millimeters with the strong electric field variations. These variations are amplified by the polarization.

4.3. Poloidal Velocity estimation

The poloidal velocity is computed across all the radial positions for both probes. Since the results are redundant, only the velocity for probe 1 will be presented. The estimation is obtained using the method described in Chapter 2.4.

The sobreposition between the results obtained from both methods is presented:

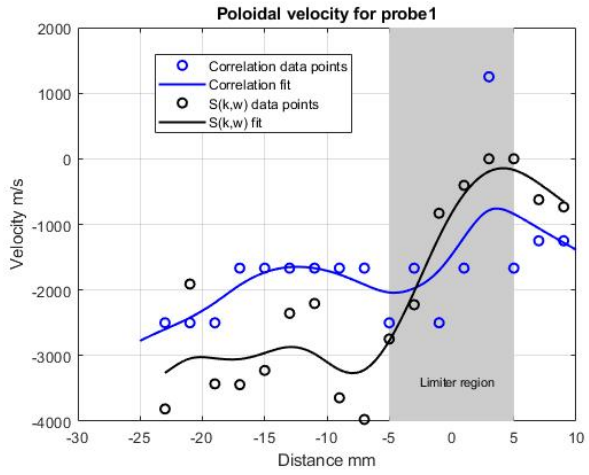

Figure 7: Plasma Poloidal velocity for probe 1 with B=0.5.

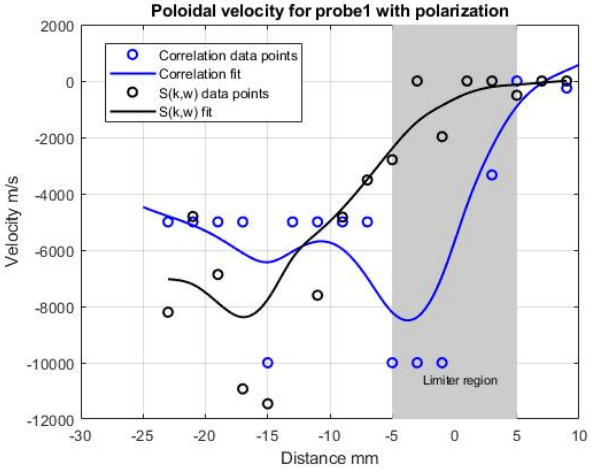

Figure 8: Plasma Poloidal velocity for probe 1 with B=0.5 .

The radial profiles, presented in Figures 7 and 8 confirm the increase in poloidal velocity as we start to move into the innermost regions of the tokamak. Both polarized and nonpolarized signals show this profile, with polarization being characterized by much higher speeds. The poloidal velocity varies slowly in the SOL region. Strong velocity gradients are observed after the limiter, which can be explained by a strong shear layer. This shear is stronger in the polarization experiment, which is why the poloidal velocitis during polarization are usually much higher.

The analysis of probe 1 suggests that the poloidal velocity stabilizes after the 10/15mm mark inside the limiter, for both polarized and no polarized plasma, with osculating values of velocity.

The signals from the experiment with a higher magnetic field configuration are also studied. The

same profile is observed, with the poloidal velocity increasing after the limiter region. The velocity decreases between the 10 and 15 millimeter region, with values around 500m/s. After this, the velocity increases again, with values up to 2000m/s.

All quantities analyzed through this work, with the exception of poloidal velocity, show big variations between the radial positions 10/15 millimeters inside the limiter, which would suggest that the shear layer is around that radial position. From the results of the poloidal velocity, using the S(k,w) method, that shear layer seem to be located right after the limiter, with velocity increasing fast.

The correlation method confirms the increasing plasma poloidal velocity moving into the inner regions of the tokamak. In this analysis, the velocity do not vary much moving from the SOL to the limiter, as we have seen in the previous method.

4.4. Reynolds Stress

The Reynolds Stress, also known as a turbulent flux of momentum, introduced in section 2.2 is explored using the signals from the Langmuir probe array. This mechanism is intrinsically related to the generation of shear flows by turbulence, so the values around the SOL are expected to be close to zero.

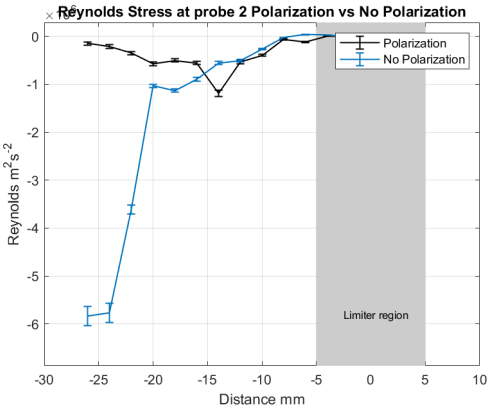

Figure 9: Reynolds Stress radial profile for probe 2.

The Reynolds stress results, presented in Figure 9 stay around zero until the position 10/15 millimeters inside the limiter. After, the non-polarized results for the Reynolds Stress increase rapidly. Unfortunately, due to the lack of points in inner regions, due to limitations when working with Langmuir probes, there is no way to tell if the Reynolds keeps decreasing or not after the 26-millimeter mark. These results show a clear effect of the polarization on turbulence mechanisms, suppressing the Reynolds stress, keeping this flux of momentum almost constant at all radial positions. Higher magnetic field seem to increase the shear, decorrelating the turbulent events. The effect is not so visible as in the case of applying polarization, but there is a clear decrease in the Reynolds stress, comparing the non polarized plasma.

Following the statistical analysis, the Reynolds Stress power spectrum is calculated:

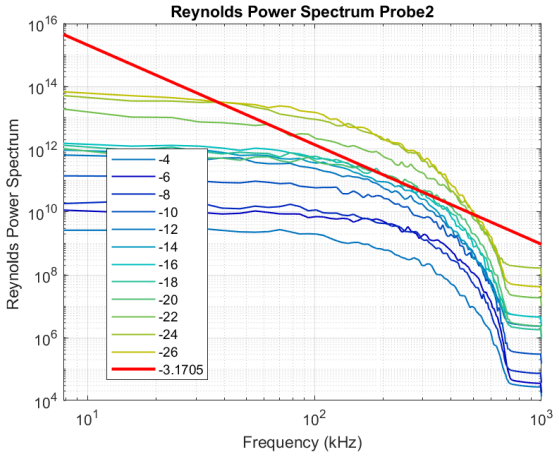

Figure 10: Reynolds power spectrum for probe 2. Positive Cycle

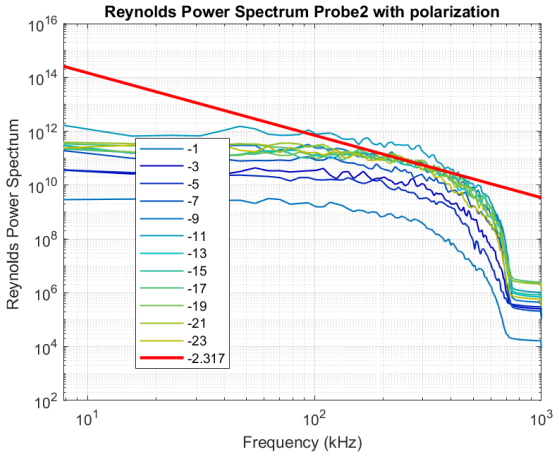

Figure 11: Reynolds power spectrum for probe 2 with polarization. Positive Cycle

The Reynolds Stress power spectrum for the non polarized plasma at Figure 10 show a spectral index of about 3.8. The polarization results at Figure 11 seem to slow down the exponential decay on the power spectra with spectral indexes values 20% and 27% lower than the ones without polarization.

4.5. $E \times B$ particle flux

The results for the particle flux are presented in Figure 12:

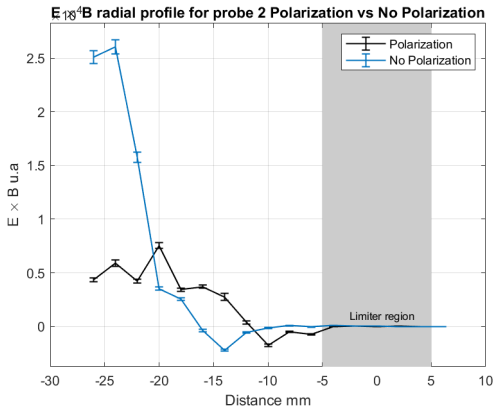

Figure 12: $E \times B$ flux radial profile for probe 2. Positive Cycle.

Values of particle transport close to zero in the SOL and limiter region are observed, where plasma is less dense, with values increasing in the inner regions. Just like in the case of the Reynolds profiles, the particle flux seems to be suppressed after applying polarization to the plasma. This suppression is also detected for the higher magnetic field configuration. The increasing particle flux moving inwards is still visible. Although, the absolute values of the particle flux show a major decrease, comparing to the results obtained for B=0.5 Tesla. The particle flux for the power spectrum yields:

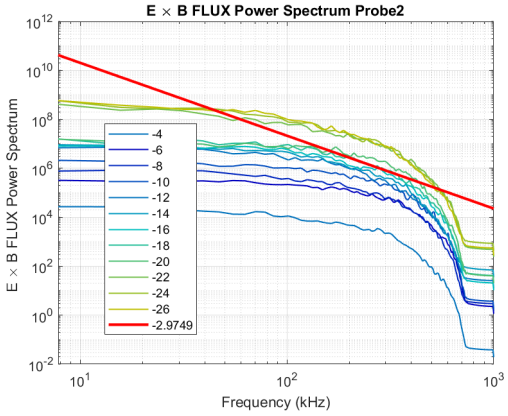

Figure 13: E × B flux for probe 2.Positive Cycle

The results from Figure 14 show consistently a decrease in the spectral index for the polarization results. The experiment with higher magnetic field applied, shows a comparable behavior with the polarization results.

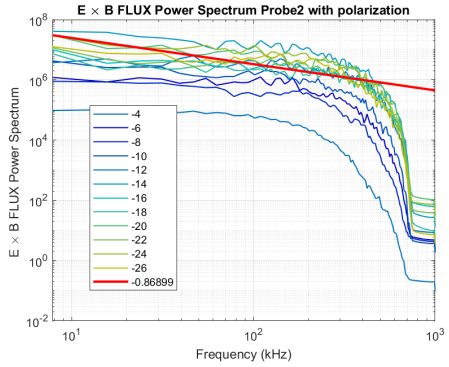

Figure 14: E × B flux for probe 2 with polarization.

4.6. Vorticity

The vorticity, presented in Section 2, is computed using the floating potential signals acquired with the Langmuir probe array. The vorticity radial profile results for the first experiment are presented in Figure 15:

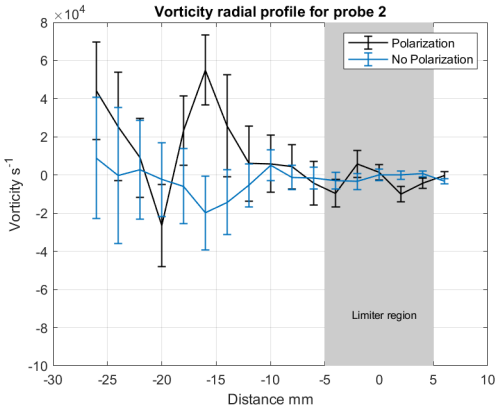

Figure 15: Vorticity radial profile for probe 2. Positive Cycle.

The vorticity in the plasma outer region is characterized by fluctuations around zero, and strong variations after the 10/15 millimeter mark. Both profiles from the first and the second experiment, without the influence of the electrode, show similar behavior. The vorticity is computed with floating potential signals as introduced in equation 4 and it is directly related to turbulence. Inner regions of the tokamak, with higher turbulence, are associated with stronger variations in vorticity as expected. The polarization introduces even bigger variations, which may be associated with a stronger shear layer generated by it. For probe 1, the vorticity grew from $-3 \times 10^4 s^{-1}$ to about $5 \times 10^4 s^{-1}$ between the radial positions [-20mm -22mm]. This result can be compared with the bigger variation during the non-polarized interval, which occurred between the same positions and has values between $-2.5 \times 10^4 s^{-1}$ to

about $-5.8 \times 10^4 s^{-1}$. The variation with the introduction of polarization is 40% times bigger in this specific interval. In general, all radial variation on vorticity where much stronger for the polarized intervals.

A higher magnetic field is associated with lower fluctuations on vorticity. The stronger variations in vorticity for the third experiment can be detected between 10 and 20 millimeter region inside the limiter.

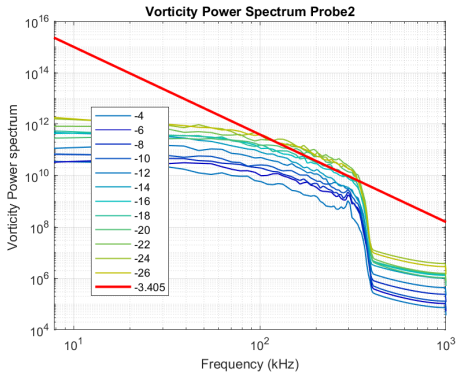

Figure 16: Vorticity power spectrum for probe 2. Positive Cycle

The vorticity power spectrum is performed through all signals after the limiter, and it is presented in Figure 16 and 17 . The power spectrum in SOL is weaker and more affected by the acquisition system noise, not being represented here. The results for the vorticity power spectra are presented. Worth noticing that the results are plotted in a logarithmic scale, so the fitted line corresponds to the decay factor, also known as spectral index:

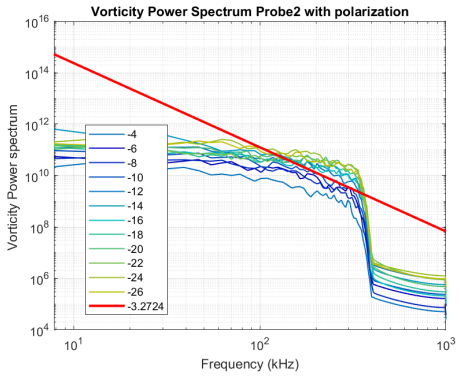

Figure 17: Vorticity power spectrum for probe 2 with polarization. Positive Cycle

The exponential decay is confirmed in the previous results, giving a spectral index for vorticity around -4 for probe 1 and -3.4 for probe 2. There is some evidence that the polarization decreases the decay rate of the presented turbulent process, with decays of -3 and -3.2 for probe 1 and probe 2 respectively.

The vorticity flux, previously introduced in equation 5 is computed:

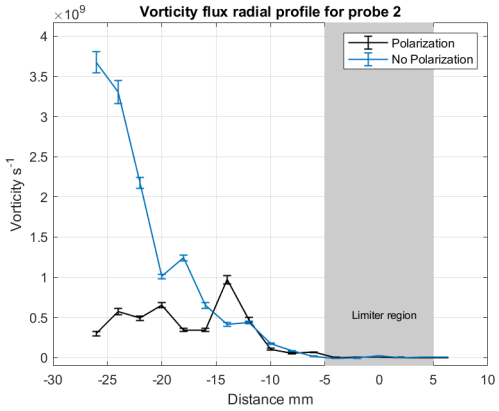

Figure 18: Vorticity flux radial profile for probe 2. Positive Cycle.

The vorticity flux, presented in Figure 18 is close to zero until 15 millimeters into the limiter. After, high flux values are observed with a maximum value close $4 \times 10^9 ms^{-2}$ for probe 2. The magnitude and radial profile for all experiments are comparable. The polarization reduces the vorticity flux dramatically in the inner regions, with a maximum value close to $1 \times 10^9 ms^{-2}$ for both probes. The maximum value of vorticity flux occurs 14 millimeters inside the limiter for probe 2. The major decrease in the flux is associated with the stronger shear layer generated by the polarization in this region. The strong shear layer de-correlates the turbulent events, reducing the vorticity flux up to 90% across the most inner studied regions of the tokamak. The same increase in the shear layer happens when looking at higher magnetic field configurations. The higher magnetic field configuration suggested a decrease in the vorticity flux in inner regions of the plasma, without the polarization. The results again can be compared to the ones with polarization for the first experiment, that shows fluxes up to 10 times smaller, comparing to the non polarization results.

The higher magnetic field configuration suggested a decrease in the vorticity flux in inner regions of the plasma, without the polarization. The results again can be compared to the ones with polarization for the first experiment, that shows fluxes up to 10 times smaller, comparing to the non polarization results.

The vorticity flux power spectrum is presented in Figure 19 and Figure 20 for the non polarization and polarization results respectively:

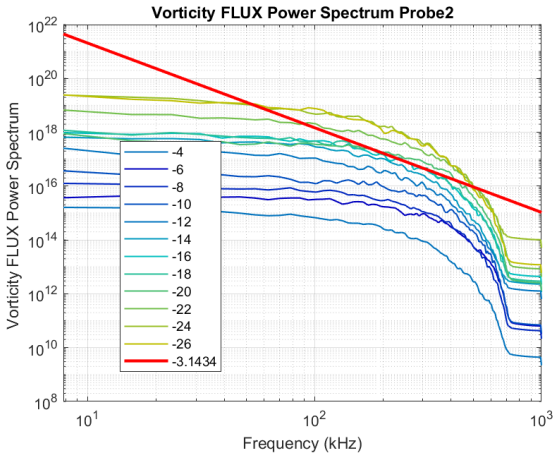

Figure 19: Vorticity flux power spectrum for probe 2. Positive Cycle

For both probes, the polarization results have lower spectral indexes. The power spectrum's without the electrode agree with the results from the first experiment, with a spectral index around 3.

There is no evidence that increasing the magnetic field increases the rate of the decay with frequency, with a spectral index of 3.21.

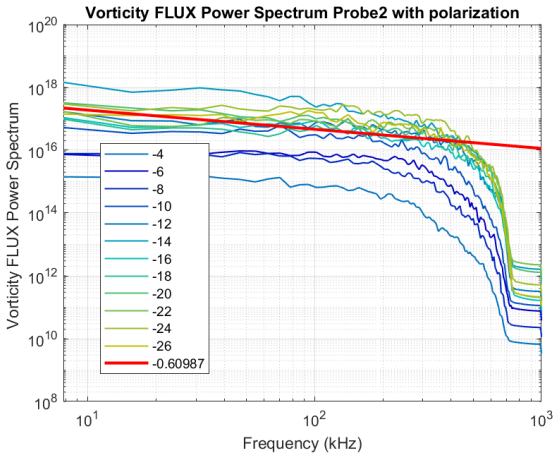

Figure 20: Vorticity flux power spectrum for probe 2 with polarization. Positive Cycle

4.6.1 Vorticity power distribution function

The vorticity data for each radial position and each probe is fitted to a Q-Tsallis, introduced in Chapter 2. The experimental data fit from the polarized and non polarized signals are presented for two radial positions as example:

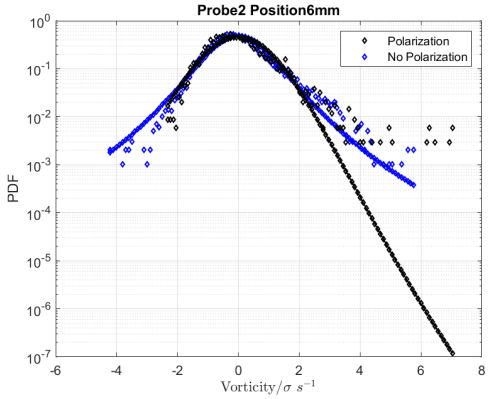

Figure 21: Q-Guassian for probe 2 at +0mm position. Positive cycle.

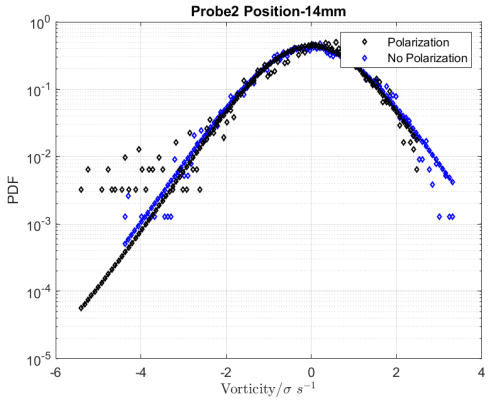

Figure 22: Q-Guassian for probe 2 at -14mm position. Positive cycle.

Inside the limiter, with the distribution skewness turning negative, and kurtosis values around 4, distributions without symmetry and skewed to the left are expected.

The Q-Gaussian fit, with all the radial positions under analysis is presented:

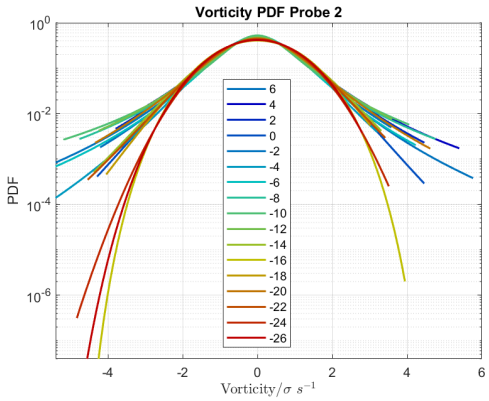

Figure 23: Q Gaussian for probe 2.Normalized values.

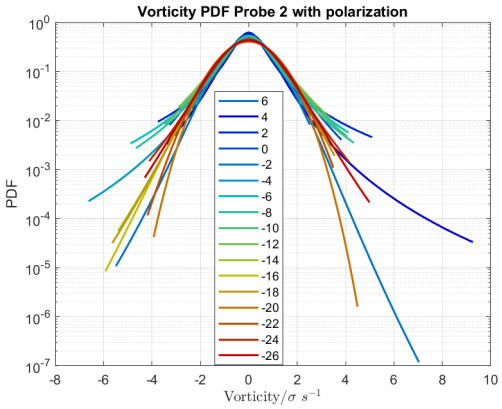

Figure 24: Q Gaussian for probe 2 with polarization. Normalized values.

The darker blue fits in Figure 23 and Figure 24, represent the PDF of vorticity in the SOL region, with pronounced tails to the right. The distribution tails move to the left as we move into the inner regions of the tokamak.

The vorticity PDFs become broader as we move from the SOL to the edge regions of the plasma. The PDF tails are typical of strongly correlated systems, implying the existence of intermittent coherent structures.

5. Conclusions

The main goal of this thesis was to experimentally estimate the vorticity on ISTTOK tokamak, using a Langmuir probe array.

The results show that the vorticity flux may strongly contribute to the shear flow amplification in the plasma edge region. The particle flux and vorticity flux are closely related during all experiments.

It was observed that the vorticity is constant in the SOL and limiter region but in the plasma edge, where the ExB shear flow is higher a larger dispersion is observed in the vorticity measurements. The observed dispersion is not unexpected as theoretical models have predicted that the magnitude of the shear layer leads to selectivity of the vorticity [2]. In this work it was shown that in the absence of the sheared flow, the axial (perpendicular to the plane) vorticity field would be rather homogeneous and isotropic while a sheared flow carries an associated constant axial vorticity that is added to the background vorticity. The vorticity is well fitted by a Q-Gaussian distribution, with flattened distributions and heavier tails for inner positions, and sharper distributions for outer regions. The PDF tails are typical of strongly correlated systems, implying the existence of intermittent coherent structures.

The poloidal velocity increases as we move into inner radial positions of the tokamak. All the results, from both methods agree that the poloidal velocity in the SOL region show little variations along the radial positions analyzed. Strong variations in the poloidal velocity are observed in inner regions, around 5 millimeters inside the limiter with the S(k,w) and correlation method. Poloidal velocity is also affected by the polarization, with much higher velocities in the inner regions of the tokamak. All the previous mentioned results confirm the presence of the shear layer, and the amplification of it with polarization.

Experiments with higher magnetic field also show impact on the confinement conditions as expected, with lower values of Reynolds stress, particle flux, vorticity flux and vorticity. This results can be compared to the ones from the plasma signals with polarization.

References

[1] H. Bigliari et al. Radio frequency power in plasmas. *AIP Conf. Proc. No. 244(AIP, New York*, page 376.

[2] R. Sanchez et al . Plasm. phys. control. fusion 53. 2011.

[3] Bruno Gonçalves and I. Henriques and C. Hidalgo and C. Silva and H. Figueiredo and V. Naulin and A H. Nielsen and J.T. Mendonça. *Radial structure of vorticity in the plasma boundary of ISTTOK tokamak*, 2018.

[4] Burton, W.B. and Kuijpers, J. and Heuvel, Edward and Laan, H. and Appenzeller, I. and Bahcall, J. and Bertola, F. and Cassinelli, Joseph and Cesarsky, C. and Engvold, O. and McCray, R. and Murdin, P. and Pacini, F. and Radhakrishnan, V. and Sato, K. and Shu, F. and Somov, B. and Sunyaev, R. and Tanaka, Y. and Kaw, Predhiman. *Nonequilibrium Phenomena in Plasmas*. 01 2005.

[5] C. Hidalgo and C. Silva and M. A. Pedrosa and E. Sánchez and H. Fernandes . Radial structure of reynolds stress in the plasma boundary of tokamak plasmas. *Physical review letters*, 83(11), Sept. 1999.

[6] Dinklage, A., Klinger, Th., Marx, G., Schweikhard, L. (Eds.). Plasma physics confinement, transport and collective effects. pages Springer–Verlag Berlin Heidelberg.

[7] Freedman David, Diaconis Persi . On the histogram as a density estimator: L2 theory. *Probability Theory and Related Fields*, 57:453–476, 1981.

[8] G. G. Craddock and P. H. Diamond. *Phys. Rev. Lett*, 67(1535), 1991.

[9] J.M. Beall and Y.C. Kim and E.J. Powers. Estimation of wavenumber and frequency spectra using fixed probe pairs. *Department of Electrical Engineering and Electronics Research Center, The University of Texas at Austin, Austin, Texas*, 1981.

[10] Kat, Roeland and Ganapathisubramani, Bharathram. Frequency–wavenumber mapping in turbulent shear flows. *Journal of Fluid Mechanics*, 783:166–190, 11 2015.

[11] S.B. Korsholm and P.K. Michelsen and colleges. Reynolds stress and shear flow generation. *Plasma Phys. Control. Fusion*, 43:1377–1395, 2001.

[12] Sousa-Silva, Carlos and Figueiredo, H. and Nedzelskiy, I. and Gonçalves, Bruno and Varandas, Carlos. Control of the edge turbulent transport by emissive electrode biasing on the tokamak isttok. *Plasma Physics and Controlled Fusion*, 48:727, 04 2006.

[13] Sérgio Caramona. *Design and exploitation of a vorticity probe for turbulence studies in fusion devices*. IST, 2020. Master Thesis.